Investigation of dosimetry in human head model for a helical antenna with mobile phone

Article *in* International Journal of Physical Sciences · March 2011

CITATIONS
16

READS
230

5 authors, including:

Norbahiah Misran
Universiti Kebangsaan Malaysia
142 PUBLICATIONS **1,633** CITATIONS
SEE PROFILE

Mohammad Rashed Faruque
Universiti Kebangsaan Malaysia, UKM, Bangi
399 PUBLICATIONS **3,735** CITATIONS
SEE PROFILE

Mohammad Tariqul Islam
Universiti Kebangsaan Malaysia
1,222 PUBLICATIONS **11,626** CITATIONS
SEE PROFILE

International Journal of the Physical Sciences Vol. 6(5), pp. 1000–1008, 4 March, 2011
Available online at http://www.academicjournals.org/IJPS
DOI: 10.5897/IJPS10.446
ISSN 1992 - 1950 ©2011 Academic Journals

Full Length Research Paper

Investigation of dosimetry in human head model for a helical antenna with mobile phone

Norbahiah Misran[1,2], Mohammad Rashed Iqbal Faruque[1,2]*, Mohammad Tariqul Islam[1] and Hafizah Zoinool Abidin[1,2]

[1]Institute of Space Science (ANGKASA), Universiti Kebangsaan Malaysia 43600 UKM, Bangi, Selangor, Malaysia.
[2]Department. of Electrical, Electronic and Systems Engineering, Faculty of Engineering and Built Environment, Universiti Kebangsaan Malaysia 43600 UKM, Bangi, Selangor, Malaysia.

Accepted 18 February, 2011

This paper proposes a dosimetric analysis in realistic human head model for a helical antenna with phone model. The finite-difference time-domain (FDTD) method with lossy-Drude model is adopted in this study. The technique of SAR measurement is addressed and then the effects of head model size on SAR characteristics for a cellular phone exposure at 835 MHz respectively. The head model, was developed from magnetic resonance imaging (MRI) data of an adult head, consists of 630 thousand voxels, of 2 mm dimensions, segmented into 15 tissue types. The helical antenna was modeled as a heap of dipoles and loops with a sufficient relative weight, whose legality was established by comparing the calculated near magnetic fields with published measured data. SAR is given for both the spatial peak value in the whole head and the averages in various major organs.

Key words: Specific absorption rate (SAR), head size, helical antenna, finite difference time domain method (FDTD), electromagnetic dosimetry.

INTRODUCTION

The trend to smaller devices with increased complexity (that is, multipurpose devices with multiple mobile bands including bluetooth and WLAN data connectivity) continuously increases the challenges for RF and product engineers and designers. The radiation performance of such complex small devices is also getting more sensitive with respect to the proximity to the hand and, in particular, to the head since antenna and head grip can no longer be spatially separated. This has also heightened the fears of service providers that over-the-air performance of phones may be insufficient and they have requested that head models be included in the next revision of the standards (IEEE C95.1-2005, 2005; ICNIRP Guidelines, 1988; Christopoulou et al., 2009; Ebrahimi-Ganjah et al., 2007).

The health effects of the EM waves on the human body are dependent on the frequency and strength of the waves (ICNIRP Guidelines, 1988). In particular, above 100 kHz, the absorbed EM energy mainly contributes to tissue heating. The basic parameter in the EM dosimetry is defined in terms of the specific absorption rate (SAR), or the absorbed powered in unit mass of tissue (Ebrahimi-Ganjah et al., 2007; Kouveliotis et al., 2006). The SAR has been used as the standard dosimetric parameter for EM wave exposure (ICNIRP Guidelines, 1988; Christopoulou et al., 2009). Therefore, the SAR evaluation of EM waves is an important research topic that needs to be taken into consideration by the World Health Organization (WHO), Geneva, Switzerland (ICNIRP Guidelines, 1988).

The original form of the helical antenna was developed by Kraus in 1946 and radiated a circularly polarized field from the end of the antenna, this being termed the axial or end fire mode of operation (Kunz and Luebbers, 1993). To achieve this mode of operation the diameter of the helical and the spacing between the loops must be large fractions of a wavelength, with an optimum circumference of approximately 1λ for circular polarization. Some of the proposed satellite based personal communications systems will use circular polarization and human proximity effects on circular polarized helical antennas were recently analyzed using the method of moments

*Corresponding author. E-mail: rashedgen@yahoo.com.

(M_OM) and the finite-difference time-domain (FDTD) method (Kouveliotis et al., 2006; Kunz and Luebbers, 1993; Balzano et al., 1995; Wang and Fujiwara, 1999).

An approach to FDTD modeling of normal-mode helical antennas was recently proposed whereby the helical is approximated by a series of small loops and dipoles with source weights derived from analytical expressions for the helical far-fields (Lazzi and Ghandhi, 1998; Okoniewski and Stuchly, 1996; Hombach et al., 19960. Good agreement with experimental measurements for near electric field measurements, far-field radiation patterns and induced specific absorption rate (SAR) was reported. However, that method does not provide information on the input impedance of the helix and requires access to the FDTD source code to modify the excitation subroutines. This method adapts very well to the human head models which are usually derived from magnetic resonance imaging (MRI) or computed tomography (CT) scans and offers great litheness in modeling the heterogeneous structures of anatomical tissues and organs. The MRI or CT based western various types of head models have been reported (Okoniewski and Stuchly, 1996; Hombach et al., 1996; Dimbylow, 1997; Gabriel, 1996). An anatomically realistic head model is indispensable for a detailed dosimetric analysis.

However, few dosimetric analyses have been addressed in the literature. This is because an obvious difficulty is the modeling of helical using usually rectangular FDTD cells. Lazzi and Gandhi have recently proposed a method to model a helical antenna as a stack of dipoles and loops, which does not need modification of the FDTD cell resolution to represent the helical or curved metal wires (Lazzi and Ghandhi, 1998).

A dosimetric analysis is performed in a newly developed MRI-based head model for an actual mobile telephone with helical antenna in this paper. The mobile telephone is modeled as a plastic covered metal box and the helical antenna is modeled by using the Lazzi and Gandhi proposed method. The validity for the actual mobile telephone modeling is first confirmed by comparing the calculated near magnetic fields with measured data published in the literature. Then SAR are given both for the spatial peak value in the whole head and the averages in various major organs. Taking into consideration that a mobile telephone may not be adequately metalized a dosimetric analysis for a plastic covered abridged metal box with the same helical antenna is also carry out.

NUMERICAL METHOD

Simulations using CST Microwave Studio, a commercially available software package have also been carried out (Islam et al., 2009, 2009b, 2010). A rectangular computational grid, based on the Yee cell, with a resolution of 1.25 mm and the total-field formulation have been used, while the perfectly matched layer (PML) absorbing boundary conditions with 8 PML has been employed (Islam et al., 2009; Kuster and Balzano, 1992; Okoniewski and Stuchly, 1988). The boundaries were placed 30 cells away from the nearest scattered. Converged results have been assured by using 12 time periods. The helical geometry has been approximated in the FDTD grid as a rectangular helical of wires using perfect conducting cell edges. The excitation has been modeled by imposing a harmonic voltage at a vertical one-cell feeding gap. The current flowing through the voltage source cell has been calculated by integrating the magnetic fields around the voltage source according to Ampere's law. The input impedance of the antenna has then been derived from the ratio of the voltage and the current together with their phase difference.

Averaged SAR over a reference mass (1 or 10 gm) is calculated by an interpolation scheme. Cubical spaces centered on a cell are formed and the mass and average SAR of the sample cubes are found. The size of the sample cube increases until the total enclosed mass exceeds the reference mass. The sample cube increases in odd-numbered steps (1×1×1, 3×3×3, 5×5×5 etc.) to remain centered on the desired cell. The cube may contain some non tissue cells, but it cannot contain an entire side or corner of non tissue cells. If the cube is found to be invalid, the averaging for the center cell stops and the same procedure is performed for the next center cell.

HEAD MODELS

In this study, we present a MRI-based, high-resolution, numerical model of the head of a healthy human subject. In order to devise the model, we performed quantitative volumetric segmentation on the human head, using T1-weighted MRI. The high special resolution used (1 × 1 × 1 mm^3), allowed for the precise computation and visualization of a higher number of anatomical structures than provided by previous models. Furthermore, the high spatial resolution allowed us to study human being thin anatomical structures of clinical significance not visible by the standard model currently adopted in computational bioelectromagnetics. When we computed the electromagnetic field and specific absorption rate (SAR) at 7 Tesla MRI using the high-resolution model, we were able to obtain a detailed visualization of such fine anatomical structures as the epidermis/dermis, bone structures, bone-marrow, white matter, and nasal and eye structures. An MRI based head mode laws utilized by software recently (Dimbylow, 1997).The raw MRI data were taken from an adult head (male, 23 years old), which consists of 115 slices with 2 mm apart in the axial plane. Each MRI slice was a 256× 256 pixel and 9-bit grey scale image. The grey scale data of MRI images were interpreted into tissue types, which are known as a process of segmentation. The segmented tissue types are blood, bone, bone marrow, cartilage, cerebrospinal fluid (CSF), dura, eye tissue, fat, grey matter, lens, mucous membrane, muscle, parotid gland, Skin and white matter.

Figure 1 shows the head model, a midsagittal vertical cross-section and a horizontal cross-section through the eyes of the head model. The electrical properties for each tissue are cited from (Gabriel, 1996) and tabulated in Table 1, where ρ is the mass density, and ε_r and σ are the relative permittivity and conductivity, respectively.

HELICAL ANTENNAS WITH PHONE MODEL

A small diameter (compared to wavelength) helical antenna working in the normal mode and a series of equivalent loops and dipoles are shown in Figure 2(a) and (b), respectively. A genuine 900 MHz mobile phone, reported in (Hombach et al., 1996), was modeled by a helical antenna mounted on a plastic covered rectangular metal box. Figure 3 shows the mobile telephone with a helical antenna

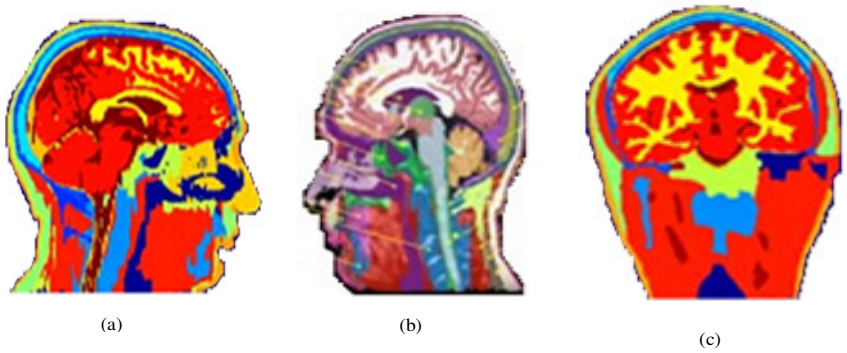

Figure 1. MRI based human head model. (a) Appearance (b) midsagittal vertical cross-section (c) horizontal cross-section through the eyes.

Table 1. Dielectric tissue properties at 835 MHz.

Tissue	ρ [kg/m^3]	ε_r	σ [S/m]
Blood	1060	61.38	1.56
Bone	1850	16.68	0.25
Bone marrow	1030	11.31	0.24
Cartilage	1100	42.71	0.81
Cerebrospinal fluid	1010	68.67	2.44
Dura	1030	44.48	0.99
Eye tissue	1010	55.29	1.21
Fat	920	11.37	0.11
Grey matter	1030	52.76	0.96
Lens	1100	41.25	0.67
Mucous membrane	1010	46.12	0.88
Muscle	1040	55.99	0.99
Parotid gland	1050	60.75	1.24
Skin	1010	41.48	0.89
White matter	1030	38.96	0.61

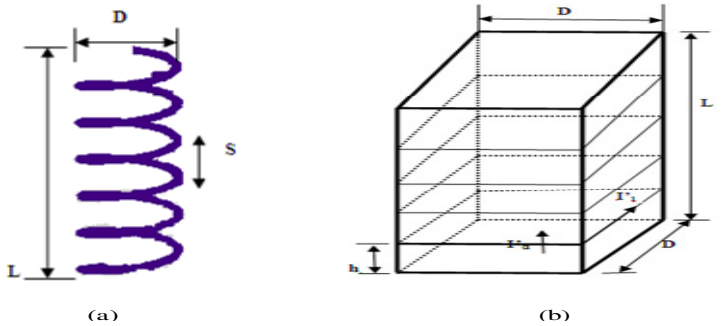

Figure 2. (a) The equivalence of a “normal mode” helical antenna in sequence of loops and dipoles (b) stack used to model the helical antenna. The stack is composed of several layers. Each layer has a square area with one side equal to the diameter D of the helical antenna, and a height h equal or close to the pitch S of the helical antenna. The height of the stack is equal to the length L of the helical antenna.

model. The phone model metal box was 5.1 cm wide, 2.2 cm thick, 13.6 cm tall, and the covered plastic case had a thickness of 2 mm and ε_r = 2. The helical antenna had a length L =18 mm, pitch S = 2 mm, diameter D = 4 mm, and was located at the onward side on

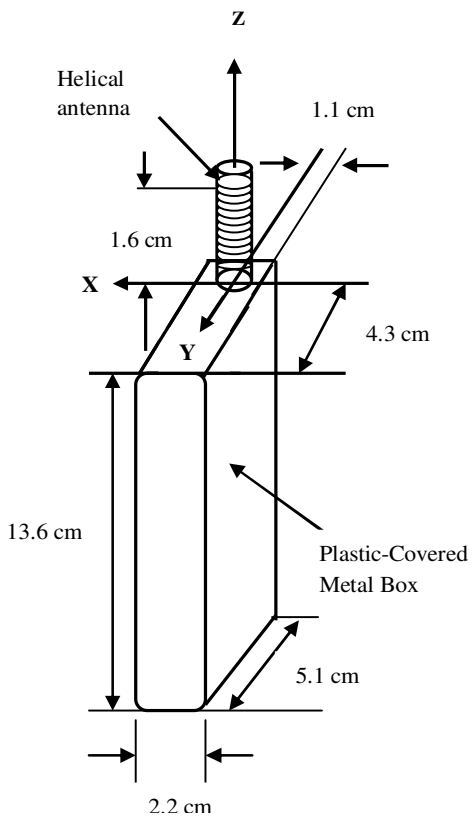

Figure 3. Model of cellular phone with a helical antenna.

the box. As in (Koulouridis and Nikita, 2004), the far field can be calculated, therefore, considering as source only one loop and one dipole. Defining η as the characteristic impedance and k the propagation constant of the free-space, we can write

$$E_\theta(r) = j\eta k I_d S \frac{\sin\theta}{4\pi r} e^{-jkr}. \quad (1)$$

$$E_\phi(r) = \eta k I_l S \frac{\pi^2 D^2}{2\lambda} \frac{\sin\theta}{4\pi r} e^{-jkr}. \quad (2)$$

where, according to Figure 2(a), D is the diameter of the helical antenna, S is the pitch, and I_d, I_l are the currents passing, respectively, through the dipole and the loop. Therefore, in the far field we have:

$$\frac{E_\theta}{E_\phi} = j\frac{I_d}{I_l}\frac{2S\lambda}{\pi^2 D^2} = j\frac{2S\lambda}{\pi^2 D^2}. \quad (3)$$

because of the continuity of the current $I_d = I_l$.

Figure 2(b) shows that for one layer of the stack, there are an equivalent dipole and an equivalent loop. Denoting the current in the equivalent dipole as I'_d, I'_d can be replaced by a displacement current, and the equivalent electric field E_z in lieu of I'_d can be expressed as:

$$E_z = \frac{I'_d . 1/j\omega C}{h} = \frac{I'_d}{j\omega\varepsilon_0 D^2}. \quad (4)$$

where, C is the capacitance between the layer, being given by $\varepsilon_0 D^2 / h$, and h is the height of each layer.

On the other hand, denoting the current in the equivalent loop as I'_l, from Ampere's law, the equivalent magnetic field related to the current I'_l in the center of the same layer can be expressed as:

$$H_z = \oint \frac{I'_l dl' \sin\phi}{4\pi R^2} \approx \frac{I'_l}{D}. \quad (5)$$

where, R is the distance from the current element dl' to the center of the layer, ϕ is the angle between the direction of the current and the vector from the element to the center of the layer, and the integration is carried out along the boundary line of the layer. Thus, for one layer of the stack, we have:

$$\frac{E_z}{H_z} = \frac{I'_d}{I'_l} . \frac{1}{j\omega\varepsilon_0 D}. \quad (6)$$

Since the stack has a rectangular shape and the height h of each layer may not be identical to the pitch of the helical antenna, it is necessary to relate the currents I'_d and I'_l to I_d and I_l produced by the actual dipole and loop. This was realized by scaling the dipole current by the ratio of the actual and modeled dipole length sand the loop current by the ratio of the actual and the modeled loop perimeters. Accordingly, we have,

$$I'_d = I_d \frac{S}{h} \text{ and } I'_l = I_l \frac{\pi D}{4D}. \quad (7)$$

Thus Equation (6) can be rewritten as:

$$\frac{E_z}{H_z} = \frac{4S}{j\omega\varepsilon_0 \pi h D}. \quad (8)$$

Since $I_d = I_l$. This equation gives the relative weight between the electric and magnetic sources as the excitation.

It is straight forward to model the stack using FDTD cells. In this study, 2× 2 cells in the *xy* planes and 9 cells along the z direction were used to model the stack. That means that $S = h$, and $D = 2\delta$ in Equation (5) where δ is the size of cubical FDTD cells. E_z and H_z in the cells modeling the stack were excited sinusoidally according to the relative weight in Equation (5). Due to each layer of the stack consisted of four cells, the excitation with E_z and H_z was split and assigned as shown in Figure 4 according to Lazzi and Gandhi's proposal.

To confirm the validity of our modeling for the actual mobile telephone, the free space magnetic field *H* was calculated. Figure 5 shows calculated $|H|^2$ value at a distance of 5 mm from the cellular telephone. Also shown is the measured result reported in (Hombach et al., 1996) by using a magnetic field probe. A good agreement was observed between them, though the calculated

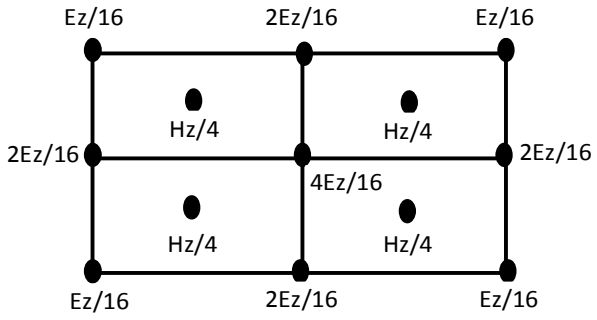

Figure 4. The excitation method for each layer of the stack modeling the helical antenna.

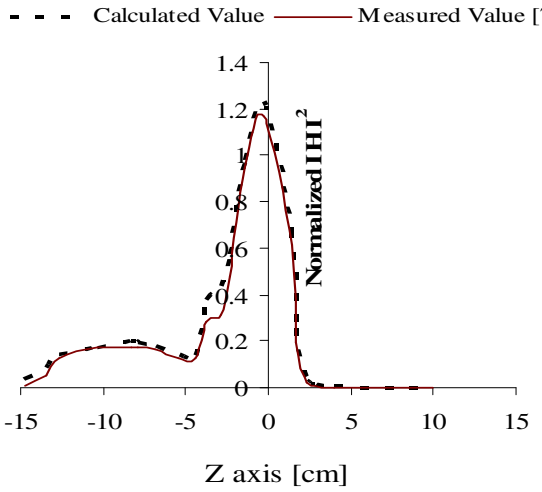

Figure 5. Calculated and measured (Balzano et al., 1995) squared magnetic fields both normalized to the maximum field values at a distance of 5 mm from the phone model.

values were somewhat larger than the measured ones on the lower part of the box. This result assured that the model is a good representation of the actual portable telephone.

RESULTS AND DISCUSSION

All calculated results are analyzed in three sections. The antenna output power was set to 0.6 W, which was obtained from the sum of the power absorbed in the head and hand and the power radiated to the far field. The radiated power was calculated by integrating the normal component of the pointing vector over a surface completely surrounding the configuration of analysis. The hand was simply modeled with 2/3 muscle equivalent material being 8 cm wide and 2 cm thick and wrapped around three sides of the lower part of the cellular telephone. The portable telephone had a vertical alignment at the side of the head by the ear.

Helical antenna on a plastic-covered metal box

The magnetic field distribution as can be seen in Figure 5, the helical antenna had stronger magnetic fields concentrated in the vicinity of the feed point. Also from Figure 5, the helical antenna did not effectively choke the RF current on the box which is directly related to the near magnetic field (Kuster and Balzano, 1992). This means that there may be an increased spatial peak SAR value in the head. Table 2 gives the SAR distributions for main organs in the MRI-based head model with the helical antenna on the plastic covered metal box. For comparison, the SAR distributions in the same MRI-based head model with a quarter-wavelength monopole antenna on a plastic covered metal box are also given. The quarter-wavelength monopole antenna had a radius of 0.48 mm and was located at the same location as that of the helical in Figure 3. Both the 1 gm averaged and the 10 gm averaged spatial peak SAR were obtained over an exact 1 or 10 gm soft issue by using a linear interpolation scheme (Wang and Fujiwara, 1999). In addition, the 1 gm averaged spatial peak SAR for the brain was obtained over 1 gm of the grey matter, white matter and CSF, and the 1 gm averaged spatial peak SAR for the eye was obtained over 1 gm of the eye tissue and lens. As expected, a raise in the 1 gm averaged and 10 gm averaged spatial peak SAR, say 1.1 times for the 1 gm average and 1.4 times for the 10 gm average, was observed with respect to the quarter-wavelength monopole. Moreover, the average SAR in the parotid gland was also increased significantly. But the average SAR in the major organs such as the brain and eyes were lower with respect to the quarter-wavelength monopole. This can be explained by comparing the SAR distributions on the head surface, as shown in Figure 6, for the two different antennas. Due to the shorter length of helical antenna, the currents concentrated on the antenna and the upper part of the box, which resulted in a concentrated EM absorption in the face area touching the ear piece of telephone. However, with respect to the helical antenna, the peak values were lower but the exposed area was larger for the helical antenna. The exposed area for the helical antenna was somewhat on the low side relative to the auditory canal, while somewhat on the high side for the helical antenna that attributed to the increased average SAR level in the parotid gland and decreased average SAR level in the brain and eyes.

It is difficult to make a direct comparison for the spatial peak SAR with those reported in (Wang and Fujiwara, 1999) because different helical sizes and different head models have been used. Lazzi and Gandhi have reported a 1 gm averaged spatial peak SAR of 3.9 W/kg at 835 MHz in (Wang and Fujiwara, 1999). This value is approximately 1.9 times our result at 835 MHz. The reason may be due to a shorter helical length and a pressed-ear head model used in their computation,

Table 2. SAR distributions for MRI-based head model. The antenna output was 0.6 W.

SAR (W/kg)	Helical	Quarter-wavelength monopole
1 gm peak SAR	2.006	1.75
10 gm peak SAR	1.16	0.82
Average SAR for whole head	0.048	0.047
1 gm peak SAR for brain	1.19	1.05
1 gm peak SAR for eye	0.022	0.032
Average SAR for grey matter	0.045	0.046
Average SAR for white matter	0.027	0.028
Average SAR for CSF	0.074	0.075
Average SAR for eye tissue	0.008	0.011
Average SAR for lens	0.002	0.005
Average SAR for parotid gland	0.119	0.087

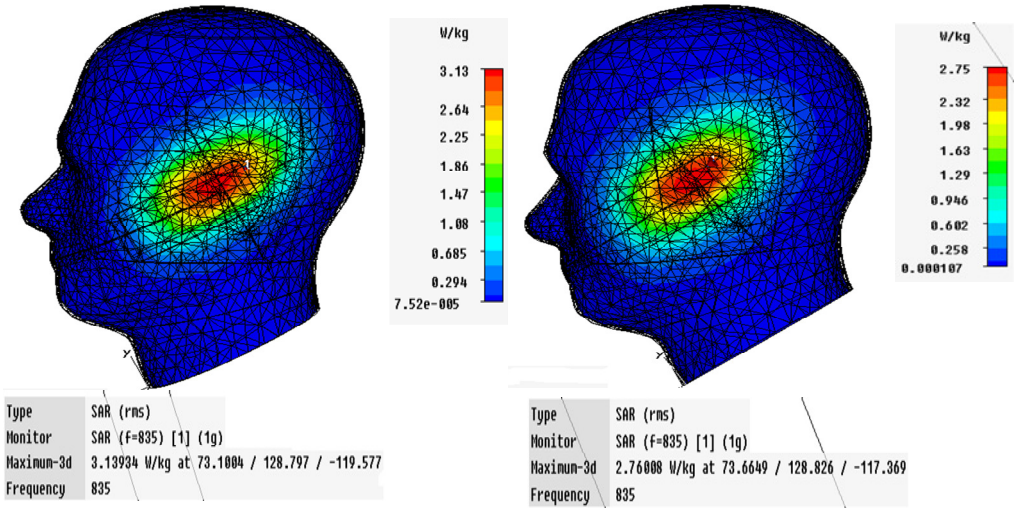

Figure 6. SAR distributions on the head surface. (a) helical antenna (b) quarter-wavelength monopole antenna. The antenna output was 0.6 W.

because pressing the ear by a portable telephone would cause a significant increase in the spatial peak SAR (Kuster and Balzano, 1992; Faruque et al., 2010a).

Helical antenna on a plastic-covered shortened metal box

In accuracy the plastic mobile telephone may not be sufficiently metalized to prevent EM fields penetrating the box. It is also possible that resonant elements may exist within the digital circuits of the device. In order to determine the effects that these circuits may have upon the SAR distributions a simulation using a shortened metal box has been carried out at 835 MHz. This box is of a similar size to that of the RF units inside a commercial mobile phone. A λ/4 monopole antenna and a helical antenna used in this study. However, the effect of shortening the box is more significant (Tinniswood et al., 1998). The shortened metal box may increase the field concentration surrounding the helical and the smaller box. Table 3 gives the SAR distributions for a helical antenna with mobile telephone with a plastic covered shortened metal box. The modeled mobile telephone had the same configuration and size as those in Figure 3, except that the metal box was shortened to a height of 4.3 cm which was a similar size to a RF unit inside a portable telephone. From Table 3, a significant increase both in the peak SAR and average SAR were found with respect to the normal metal box model. The increased factors were 1.5 and 1.8 for the 1 gm averaged and 10 gm averaged spatial peak SAR. As an exception, the SAR level in the parotid gland was lower with respect to the normal metal box. This resulted from the highly

Table 3. SAR distributions for MRI-based head model with a helical antenna on a plastic covered shortened metal box. The antenna output was 0.6 W.

1 gm peak SAR	3.13
10 gm peak SAR	2.17
Average SAR for whole head	0.073
1 gm peak SAR for brain	2.27
1gm peak SAR for eye	0.032
Average SAR for grey matter	0.091
Average SAR for white matter	0.054
Average SAR for CSF	0.154
Average SAR for eye tissue	0.011
Average SAR for lens	0.032
Average SAR for parotid gland	0.074

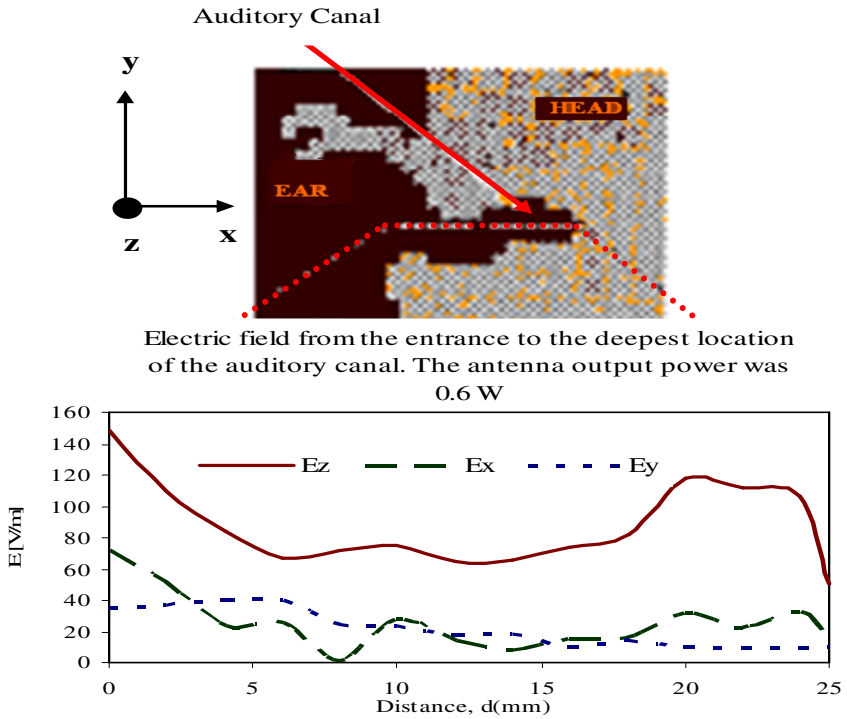

Figure 7 (a). The electric fields from the entrance to the deepest location of the auditory canal. The antenna output was 0.6 W.

field concentration and resultant smaller exposed for the portable telephone with the shortened metal box. For the cellular phone model with a normal metal box, about 33% absorbed power was due to the hand because a RF current flows on to that part of the box. However, for the mobile telephone model with the shortened metal box, only 17% absorbed power was due to the hand. The remaining part was absorbed in the head, which attributed to the increased average SAR in the head, brain and eyes. It should be noted that the radiation efficiency for the plastic covered cellular telephone model with a shortened metal box was deprived, say only 33%.

Electromagnetic fields in the auditory canal

The field attention of helical antennas in the surrounding area of the auditory canal, it is also possible that a strong field occurs deeper inside the auditory canal. This may cause the electromagnetic interference to hearing aids or artificial inner ears, especially for digital-typed mobile phones (Okoniewski and stuchly, 1988). Figure 7 shows the electric and magnetic fields from the entrance to the deepest location of the auditory canal along the x direction for the helical antenna portable telephone with a normal metal box (the model in Figure 2). As shown in

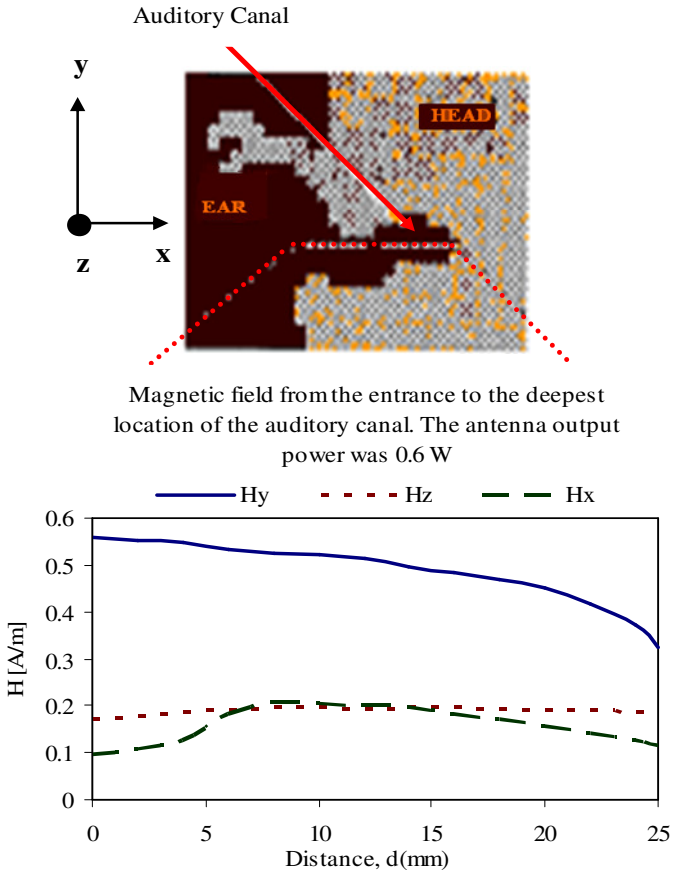

Figure 7(b). The magnetic fields from the entrance to the deepest location of the auditory canal. The antenna output was 0.6 W.

Figure 7, the electric field E_z dominated over E_x and E_y, which exhibited a standing-wave characteristic. The maximum electric field strength was found to be 148.6 V/m at the entrance of auditory canal, while a comparable strength, say 117.8 V/m, was found deeper inside the auditory canal. The magnetic fields had a dominant component H_y. H_y decreased very slowly with the distance away from the entrance of auditory canal. The maximum magnetic field strength was 0.56 A/m at the entrance of auditory canal. One general observation is that the magnitudes of the electric fields are attenuated in the ear canal, while the magnitudes of the magnetic field are enhanced. The result for the magnetic field may be surprising; however, it is in agreement with the previously reported results for a quarter-wavelength monopole antenna on a handset (Arenas et al., 2009; Wong and Wiart, 2005; Bank and Levin, 2007; Faruque et al; 2010b). The head in the near field of the handset antenna changes the input impedance and performance of the antenna. Furthermore, the fields are scattered within the heterogeneous model of the head. As a result, components of the field appear that are not present in free space. Overall, each field component may vary quite rapidly inside the ear canal, as observed in (Okoniewski and Stuchly, 1988), as well as in this paper. The magnitude of the total field usually changes more smoothly.

Certain self-consistent features of the field behavior in the ear canal can be observed. One of them is that, for the electric fields, the order of the curves for the field magnitude in the ear canal, in general, corresponds to that of the field magnitude in free space. The relationship is not evident to the same extent for the magnetic fields, but generally reasonable. The behavior of the magnetic fields is reasonable in view of the free space field distribution and previous report results.

Conclusions

A new method to model helical antennas, and generally antennas involving helical components has been presented. The helical antenna has been modeled as a stack of dipoles and loops with an adequate relative weight. As a result, a higher 1 gm averaged or 10 gm averaged spatial peak SAR has been found with respect to a quarter-wavelength monopole antenna, while lower average SAR has been found in the main organs such as the brain and eyes except for the parotid gland. The increased SAR values can be explained by the field concentration surrounding the shorter helical antenna. A plastic covered shortened metal box has exhibited a stronger field concentration effect, which results in an additional increase on the spatial peak SAR in the ear area as well as the SAR values in the brain and eyes. In addition, the electric and magnetic fields inside the auditory canal have also been investigated. The dominant component of electric field exhibits a standing-wave characteristic, while the magnetic field strength decreases with the distance away from the entrance of auditory canal quite slowly.

ACKNOWLEDGEMENTS

The authors would like to thank Institute of Space Science (ANGKASA), Universiti Kebangsaan Malaysia (UKM) and the MOSTI Secretariat, Ministry of Science, Technology and Innovation of Malaysia, e- Science fund: 01-01-02-SF0612, for sponsoring this work.

REFERENCES

Arenas JJ, Anguera J, Puente C (2009). Balanced and single-ended handset antennas: Free space and human loading comparison. Microw. Opt. Technol. Letts., 51(9): 2248-2254.

Balzano Q, Garay O, Manning TJ (1995). Electromagnetic energy exposure of simulated users of portable cellular phones. IEEE Trans. Vehicular Technol., 44: 390–403.

Christopoulou M, Koulouridis S, Nikita KS (2009). Parametric study of power absorption patterns induced in adult and child head models by small helical antennas. Progr. Electromagn. Res., PIER, 94: 49-67.

Dimbylow PJ (1997). FDTD calculations of the whole body averaged

SAR in an anatomically realistic voxel model of the human body from 1 MHz to 1 GHz. Phys. Med. Biol., 42: 479-490.
Ebrahimi-Ganjeh MA, Attari AR (2007). Interaction of dual band Helical and PIFA handset antennas with human head and hand. Progr. Electromagn. Res., PIER, 77: 225–242.
Faruque MRI, Islam MT, Misran N (2010a). Effect of human head shapes for mobile phone exposure on electromagnetic absorption. Informacije MIDEM, 40(3): 232-237.
Faruque MRI, Islam MT, Misran N (2010b). Evaluation of specific absorption rate (SAR) reduction for PIFA antenna using Metamaterials. Frequenz J., 64(7-8): 144-149.
Gabriel C (1996). Compilation of the dielectric properties of body tissues at RF and Microwave frequencies. Brooks Air Force Technical Report, Al/ OE-TR-1996-0037.
Hombach V, Meier K, Burkhardt M, Khun E, Kuster N (1996). The dependence of EM energy absorption upon human head modeling at 900 MHz. IEEE Trans. Microw. Theory Tech., 44(10): 1865-1873.
IEEE C95.1-2005 (2005). IEEE standards for safety levels with respect to human exposure to radio frequency electromagnetic fields 3 kHz to 300 GHz. Institute of Electrical and Electronics Engineers, New York, NY.
International Non-Ionizing Radiation Committee of the International Radiation Protection Association (1988). Guidelines on limits on exposure to radio frequency electromagnetic fields in the frequency range from 100 kHz to 300 GHz. Health Phys., 54(1): 115-123.
Islam MT, Faruque MRI, Misran N (2009). Design analysis of ferrite sheet attachment for SAR reduction in human head. Progr. Electromagn. Res., PIER, 98: 191-205.
Islam MT, Faruque MRI, Misran N (2010). Study of specific absorption rate (SAR) in the human head by metamaterial attachment. IEICE Electron. Express, 7(4): 240-246.
Islam MT, Faruque MRI, Misran N (2009b). Reduction of specific absorption rate (SAR) in the human head with ferrite material and Metamaterial. Progr. Electromagn. Res., PIER, C(9): 47-58.
Kouveliotis NK, Panagiotou SC, Varlamos PK, Capsalis CN (2006). Theoretical approach of the interaction between a human head model and a mobile handset helical antenna using numerical methods. Progr. Electromagn. Res., PIER, 65: 309–327.
Koulouridis S, Nikita KS (2004). Study of the coupling between human head and cellular phone helical antennas. IEEE Trans. Electromagn. Compa., 46(1): 62-70.
Kunz KS, Luebbers RJ (1993). The finite difference time domain for electromagnetics, Boca Raton, FL, CRC.
Kuster N, Balzano Q (1992). Energy absorption mechanism by biological bodies in the near field of dipole antennas above 300 MHz. IEEE Trans. Veh. Technol., 41(1): 17-23.
Lazzi G, Gandhi OP (1998). On modeling and personal dosimetry of cellular telephone helical antennas with the FDTD code. IEEE Trans. Antennas Propag., 46: 525–530.
Okoniewski M, Stuchly MA (1988). Modeling of interaction of electromagnetic fields from a cellular telephone with hearing aids. IEEE Trans. Microw. Theory Tech., 46(11): 1686-1693.
Okoniewski M, Stuchly MA (1996). A study of the handset antenna and human body interation. IEEE Trans. Microw. Theory Tech., 44(10): 1855-1864.
Tinniswood AD, Furse CM, Ghandhi OP (1998). Computations of SAR distributions for two anatomically based models of the human head using CAD files of commercial telephones and parallelized FDTD code. IEEE Trans. Antennas Propag., 46(6): 829-833.
Wang J, Fujiwara O (1999). FDTD computation of temperature rise in the human head for portable telephones. IEEE Trans. Microw. Theory Tech., 47(8): 1528-1534.
Wang J, Fujiara O (1999). Uncertainty of the one-gram averaged spatial peak SAR in human head for portable telephones due to average procedures. Trans. IEE Jpn., 119(1): 2-8.
Wong M, Wiart J (2005). Modeling of electromagnetic wave interactions with the human body. C. R. Physique (Elsevier), 6(6): 585-594.